Journal of Materials Chemistry C

Synthetic Versatility, Reaction Pathway, and Thermal Stability of Tetrahedrite Nanoparticles

Journal:	*Journal of Materials Chemistry C*
Manuscript ID	TC-ART-07-2020-003599.R1
Article Type:	Paper
Date Submitted by the Author:	15-Sep-2020

Complete List of Authors:	Fasana, Christine; Furman University, Chemistry Jensen, Mitchel; Furman University, Chemistry García Ponte, Graciela; Furman University, Chemistry MacAlister, Tyler; Furman University, Chemistry Kunkel, Grace; Hope College, Chemistry Rogers, John; Hope College, Chemistry Ochs, Andrew; Hope College, Chemistry Stevens, Daniel; Hope College, Chemistry Weller, Daniel; Michigan State University, Department of Chemical Engineering and Materials Science Morelli, Don; Michigan State University, Department of Chemical Engineering and Materials Science Anderson, Mary; Furman University, Chemistry

SCHOLARONE™
Manuscripts

Synthetic Versatility, Reaction Pathway, and Thermal Stability of Tetrahedrite Nanoparticles

Christine D. Fasana,† Mitchel S. Jensen,† Graciela E. García Ponte,† Tyler R. MacAlister,† Grace E. Kunkel,‡ John P. Rogers,‡ Andrew M. Ochs,‡ Daniel L. Stevens,‡ Daniel P. Weller,* Donald T. Morelli,* Mary E. Anderson†

† Chemistry Department, Furman University, Greenville, SC

‡ Chemistry Department, Hope College, Holland, MI

* Chemical Engineering and Materials Science Department, Michigan State University, East Lansing, MI

Abstract Copper-antimony-sulfide compounds have desirable earth-abundant compositions for application in renewable energy technologies, such as solar energy and waste heat recycling. These compounds can be synthesized by bottom-up, solution-phase techniques that are more energy and time efficient than conventional solid-state methods. Solution-phase methods typically produce nanostructured materials, which adds another dimension to control optical, electrical, and thermal material properties. This study focuses on a modified-polyol, solution-phase synthesis for tetrahedrite ($Cu_{12}Sb_4S_{13}$), a promising thermoelectric material with potential also for photovoltaic applications. To dope the tetrahedrite and tune material properties, the utility of the modified polyol synthetic approach has been demonstrated as a strategy to produce phase-pure tetrahedrite that incorporates transition metal (Fe, Co, Ni, Zn, Ag) dopants for Cu, Te dopant for Sb, and Se for S. Six of these reported tetrahedrite compounds have not previously been made by solution-phase methods. For the bottom-up formation of the tetrahedrite nanomaterials, the evolution of the chemical phases has been determined by an investigation of the reaction progress as a function

of temperature and time. Digenite ($Cu_{1.8}S$), covellite (CuS), and famatinite (Cu_3SbS_4) are identified as key intermediates and are consistently observed for both undoped and doped tetrahedrites. The effect of nanostructuring and doping tetrahedrite on thermal properties has been investigated. It was found that nanostructured undoped tetrahedrite has reduced thermal stability relative to samples made by solid-state methods, while the addition of dopants for Cu increased the thermal stability of the material. Crystallinity, composition, and nanostructure of products and intermediates were characterized by powder x-ray diffraction, scanning electron microscopy with energy dispersive x-ray spectroscopy, and transmission electron microscopy. Thermal properties were investigated by differential scanning calorimetry and thermal gravimetric analysis. This synthetic study with thermal property analysis demonstrates the potential of the modified polyol method to produce tetrahedrite and other copper-antimony-compounds for thermoelectric and photovoltaic applications.

Introduction

With earth-abundant compositions and promising thermoelectric and photovoltaic properties, copper-antimony-sulfide compounds, such as tetrahedrite ($Cu_{12}Sb_4S_{13}$), are an active area of research for integration into potential renewable energy technologies.[1-12] Tetrahedrite, in particular, has attracted significant attention in the field of thermoelectrics. Thermoelectric materials are capable of converting a heat gradient into electrical current and vice versa, and could therefore recycle waste heat. Devices incorporating these materials require no moving parts or maintenance, making them optimal for long-term use. Most thermoelectric compounds contain toxic or scarce elements, such as lead or tellurium, and have high fabrication costs. The quality of

thermoelectric materials is defined by a dimensionless figure of merit (Z), described by $Z=S^2\sigma/\kappa$, consisting of thermopower (S), electrical conductivity (σ), and thermal conductivity (κ).[1, 13, 14]

Tetrahedrite is an attractive thermoelectric material because it has an inherently low thermal conductivity, due in part to its complex unit cell[2, 15] and strong lattice anharmonicity thought to arise from interactions of Sb lone pair electrons with large amplitude copper vibrations.[16] Doping of a thermoelectric material aims to improve performance by optimizing the so-called power factor ($S^2\sigma$) while decreasing the thermal conductivity, which improve the figure of merit.[2, 17-19] Research has shown that nanostructuring further decreases this thermal conductivity by enhancing phonon scattering at interfaces.[17-21] Tetrahedrite synthesized by solid-state furnace techniques have been extensively studied.[16, 22-27] These methods are time and energy intensive, requiring 48 hours to weeks at temperatures in excess of 650 °C. This reaction time has been somewhat decreased to approximately 8 hours by methods involving mechanical alloying and reactive spark plasma sintering.[28, 29] Solution-phase methods, such as solvothermal and hot-injection techniques, require less time and lower temperature to produce tetrahedrite that is typically nanostructured.[3, 6, 9, 30-32] To control size, these procedures generally utilize ligands or surfactants, which diminish thermoelectric performance. Additionally those methods typically do not generate product on the gram-scale from a one-pot reaction. Without using surfactant or ligands, a modified polyol process has successfully produced nanostructured tetrahedrite on the gram-scale from a one-pot, one-hour reaction.[33-35] The thermoelectric performance of this material is comparable to or exceeds that of compounds made by solid-state methods,[33, 34] specifically a maximum ZT of 1.1 at 723 K was found for $Cu_{11}ZnSb_4S_{13}$.[33]

The modified polyol process herein uses metal salt precursors dissolved in a high boiling point reducing solvent, tetraethylene glycol, with sodium borohydride as an additional reducing

agent.[33-36] The first aim of this study demonstrates that the modified polyol method enables the facile inclusion of a variety of dopants at different concentrations for synthesis of tetrahedrite nanomaterials. Specifically, this research focuses on dopants for Cu and demonstrates the capability of incorporating dopants for Sb and S as well as double substitution for Cu and S. Six of the tetrahedrite compounds described herein have not previously been synthesized by solution-phase methods. Characterization by powder x-ray diffraction and energy-dispersive x-ray spectroscopy investigates crystallinity and chemical composition, respectively; while scanning electron microscopy and transmission electron microscopy examine particle shape and size. This type of general approach for compositional control and dopant incorporation is often a common limitation for solid-state and solution-phase synthetic routes. Doping of a material tunes charge carrier density, which adjusts the Fermi level in the electronic band structure to optimize the power factor necessary for its integration within energy conversion technologies. The inclusion of dopants within copper-antimony-sulfide compounds and tetrahedrite, in particular, affects the aforementioned thermoelectric properties and is pertinent to tune the band gap for integration into photovoltaic applications.[5-12]

To understand the formation of the tetrahedrite nanomaterial from the bottom-up, the second aim of this study investigates the reaction pathway as a function of time and temperature was conducted. Understanding the reaction pathway may enable finer compositional control, which is especially relevant because copper-enrichment is commonly found for synthetic tetrahedrite. Identification of intermediates is useful to realize the source of potential common impurities and prevent their presence in the desired final pure product. This information about the tetrahedrite growth within the solution-phase reaction is key to envision alternative synthetic routes to further increase the range of dopants incorporated. This foundational knowledge is not

only broadly useful to those seeking to produce tetrahedrite, but is also of interest for the synthesis of other copper-antimony-sulfide compounds.

For both thermoelectric and photovoltaic applications, it is important to understand the effect of heat on the stability of the material. It is expected that nanostructuring would decrease the melting point of the material and therefore alter thermal material properties relative to the bulk material. Samples produced by the modified polyol process to demonstrate synthetic versatility have also been characterized to explore the effect of nanostructuring and doping on their thermal properties, which is the final aim of this paper. Thermal properties are investigated herein by differential scanning calorimetry and thermal gravimetric analysis. Recently the effect of doping on the thermal properties was shown for pure tetrahedrite compounds produced by solid-state synthesis.[37] A series of samples with first row transition metals dopants for Cu were fabricated by mechanical alloying and hot pressing. It was found that the undoped sample had an endothermic transition at ~880 K. This transition was observed at higher temperatures for compounds doped with the different transition metals (x=1 for $Cu_{12-x}M_xSb_4S_{13}$). A decrease in mass was observed starting at ~850 K for all samples independent of endothermic transition.[37] Previous studies have been plagued by the presence of impurities apparent in the powder x-ray diffraction data.[23, 24] This paper is the first to investigate the thermal properties for nanostructured tetrahedrite.

Research presented herein investigates the reaction pathway and the thermal stability of tetrahedrite compounds synthesized by a modified polyol solution-phase method capable of incorporating multiple dopants with tunable compositions. Nanostructure, crystallinity, and composition are characterized by powder x-ray diffraction (XRD), scanning electron microscopy (SEM), transmission electron microscopy (TEM), and energy dispersive x-ray spectroscopy (EDS). The influences of nanoscale size and dopant incorporation on the thermal properties of

synthetic tetrahedrites are examined using differential scanning calorimetry (DSC) and thermal gravimetric analysis (TGA).

Experimental Section

Materials. For the modified polyol synthesis of tetrahedrite, the three precursors were purchased from Sigma Aldrich: copper (II) acetate monohydrate (≥ 98%), sulfur powder (99.98%), and antimony (III) acetate (≥ 99.99%). These reagents were dissolved in tetraethylene glycol (99%) and the polyol process was modified using sodium borohydride (≥ 98%), which were purchased from Alfa Aesar and Sigma Aldrich, respectively. The resulting material was isolated using anhydrous ethanol (200 proof, ACS/USP grade) obtained from Pharmco-Aaper. For the incorporation of dopants, the following precursors were obtained from Sigma Aldrich: zinc (II) acetate (99.99%), nickel (II) acetate tetrahydrate (≥ 99%), cobalt (II) acetate (99.99%), iron (III) chloride hexahydrate (≥ 98%), silver nitrate (≥ 99%), tellurium dioxide (≥ 99%). Elemental selenium powder from Baker Adamson was utilized.

Synthesis. To produce 2 grams of tetrahedrite from a one-pot reaction, precursors were added to a 1-L round-bottom flask in stoichiometric amounts: $Cu(OAc)_2 \cdot H_2O$ (3.99 g, 20.0 mmol), $Sb(OAc)_3$ (1.97 g, 6.60 mmol), and sulfur (0.694 g, 21.6 mmol). Dopants were added in stoichiometric ratios depending on the desired dopant concentration; and the precursor associated with the substituted element was reduced by the same molar ratio as the dopant being added. These precursors were dissolved in 200 mL of tetraethylene glycol, stirred, and sparged with N_2 to produce a turquoise solution. Sodium borohydride (~4 g, ~100 mmol) was sonicated in 100 mL of tetraethylene glycol and then slowly added to the solution of precursors. Upon the addition of sodium borohydride, the reaction immediately increased in temperature and became a dark brown color, indicating the rapid reduction of precursor reagents. Under a positive N_2 flow, the reaction

was heated with a ramp rate of approximately 10 °C/min to 220 °C and held for one hour. The solution was then cooled to room temperature, transferred to centrifuge tubes, and centrifuged at 5000 rpm for 10 minutes. The supernatant was discarded, and the resulting pellet of nanoparticles was washed with ethanol. This process was repeated at least three times, and the resulting nanoparticle powder was dried in a vacuum desiccator. Most nanoparticle powder samples were black or gray with the only exception being samples doped with zinc, which appeared brick-red in color.

The formation of growth intermediates was investigated as a function of temperature as well as a function of time at the optimized reaction temperature of 220 °C. The preceeding procedure was followed with variations in the hold temperatures ranging from 20-250 °C. To determine the reaction progress during the one hour hold at 220 °C, reactions held at the optimized temperature for 1 min and 30 min were run with all other procedural aspects remaining the same.

To investigate the effect of consolidating powders into dense pellets, tetrahedrite material underwent processing by spark plasma sintering (SPS) in a Calnano 211-LX Dr. Sinter Spark Plasma Sintering machine. This is a common procedure for enabling transport measurements of the fully densified material. Powders were loaded into a 10 mm graphite die, and then this die was mounted in the SPS machine. Materials were sintered in an argon atmosphere under a pressure of 40 MPa at 400 °C for 10 minutes. The consolidated pellet was removed from the SPS machine and graphite die, and lastly, the sample was sanded with fine-grit sandpaper to remove surface graphite. The resulting pellet achieved a density of approximately 95%.

Structural and Compositional Characterization. The size, shape, crystallinity, purity, and composition of the tetrahedrite nanoparticles were investigated by XRD, SEM, EDS, and TEM. The XRD patterns for each synthesized tetrahedrite sample were acquired using a Rigaku Miniflex

benchtop diffractometer with Cu Kα (30 kV and 15 mA) radiation. Patterns were collected over a *2θ* range of 10 to 65°, using a scan speed of 3° per minute and a sampling width of 0.03°. Lattice constants were calculated for each composition of the tetrahedrite and are included in Table S1. The following reference patterns were utilized for XRD data analysis: tetrahedrite[15] ($Cu_{12}Sb_4S_{13}$) PDF#01-074-0270, famatinite[38] (Cu_3SbS_4) PDF#01-07-0555, covellite[39] (CuS) PDF#03-065-3928, digenite[40] ($Cu_{1.8}S$) PDF#01-075-6407, and valentinite[41] (Sb_2O_3) PDF#00-001-0729.

To obtain EDS spectra and associated SEM images, a Hitachi TM-3000 microscope with a Bruker EDSXFlash MIN SVE detector as well as a JEOL JSM-IT200LA microscope with a JEOL JED-2300 Dry SDD EDS detector were utilized. The accelerating voltage was set at 15 kV and each sample was characterized in multiple regions (minimum of 3 sites) to evaluate homogeneity within synthesized materials. Additional SEM images were collected using a JEOL JSM-7200F-LV field emission microscope operating at 2 kV. TEM images were obtained using a Tecnai G2 20 XTWIN with an accelerating voltage of 80 kV. For EDS analysis, the powder sample was placed directly onto a carbon tape tab on an SEM stub. For SEM and TEM analysis, a suspension of nanoparticles was drop-cast from dilute ethanolic solutions onto a carbon tape tab on an SEM stub and onto a nickel TEM grid (Formvar/carbon 400 mesh), respectively.

Thermal Analysis. The thermal stability of the tetrahedrite nanoparticles were characterized by DSC and TGA over a temperature range of 325 to 825 K, using a TA Q2000 apparatus and TA Q500 instrument, respectively. For DSC, approximately 10 mg of sample were placed in graphite pans. Measurements were carried out in a nitrogen atmosphere with a heating rate of 10 K/min and a sampling time of 0.20 seconds per point. For TGA, approximately 10 mg of material were heated in nitrogen atmosphere in alumina ceramic pans on alumina ceramic hangers with a heating rate of 5 K/min and a sampling time of 2.00 seconds per point.

Results and Discussion

Synthetic Versatility

This solution-phase synthetic method for tetrahedrite is a general approach for the incorporation of a wide range of dopants with tunable compositions, permitting multiple dopants to be incorporated and producing high-purity product. While this research focused on dopants for Cu, the synthetic process also successfully incorporated dopants for Sb and S as well as double substitution for Cu and S. Characterization of powder products conducted by XRD and EDS confirmed crystallinity and quantitatively assessed chemical composition, while SEM and TEM revealed particle shape and size.

Undoped tetrahedrite was found to be phase-pure by XRD (Figure 1a) with an elemental composition determined by EDS to be $Cu_{13.4\pm0.2}Sb_{4.4\pm0.2}S_{13.0\pm0.3}$ (Table 1). For the EDS analysis, the atomic ratios were determined relative to S, which was normalized to be 13 S atoms per formula unit. Although stoichiometric amounts of starting materials were added for the formation of $Cu_{12}Sb_4S_{13}$, the tetrahedrite compound formed was always copper-enriched relative to this target composition. Naturally occurring tetrahedrite has a range of compositions for Cu and Sb, which respectively is 12-14.5 and 4-4.5.[42] Elemental analysis in the literature for tetrahedrite synthesized by both solution-phase and solid-state methods has found copper-enrichment to be quite common.[22, 33, 34, 43, 44] Therefore, the typical accepted composition range for tetrahedrite is $Cu_{12\text{-}14.5}Sb_{4\text{-}4.5}S_{13}$. Copper-enrichment is often attributed to the volatility of the sulfur; and the applied heat under positive N_2 flow used in this synthetic method may result in lost sulfur. Additionally, small amounts of sulfur dissolved in the solvent may be lost during centrifugation cleaning.

This synthetic method has successfully incorporated Zn, Ni, Co, Fe, and Ag as dopants for Cu. Although Ag is found in naturally occurring tetrahedrite minerals,[45] to the authors' knowledge it has not previously been incorporated for synthetic tetrahedrite made by solid-state or solution-phase techniques. While Zn, Ni, Co, and Fe have successfully been doped in tetrahedrite using solid-state methods,[23, 24, 26-29, 37, 46, 47] this is the first published solution-phase synthesis of Ni, Co, and Ag doped tetrahedrite. In addition to showing the inclusion of dopants, the dopant concentration can be tuned for these compositions with dopant levels of x=1 and x=2 for $Cu_{12-x}M_xSb_4S_{13}$, as shown in Figure 1b. Additionally, this tunability of dopant levels is highlighted in Figure 1a with x=2, 1.5, 1, and 0.5 for $Cu_{12-x}Zn_xSb_4S_{13}$. By XRD, these are all high-quality tetrahedrite samples without the common impurities of famatinite and digenite regularly seen in the literature for samples produced by other methods.[23, 24, 32, 46]

As determined by EDS analysis, all samples have compositions within the accepted range of tetrahedrite compositions ($Cu_{12-14.5}Sb_{4-4.5}S_{13}$). This indicates that there are not significant amorphous impurities throughout the sample (Table 1). EDS data is collected at 3 or more spots, and the uncertainties shown in Table 1 are standard deviations representing spot-to-spot differences across the samples. The average relative standard deviation for all samples is 3%, which demonstrates quantitatively that the sample has a high degree of homogeneity. Just as Cu enrichment is found to occur for the undoped tetrahedrite, similar enrichment was found by EDS for most dopants added for Cu relative to the target concentration (Table 1). The elemental ratio for Zn was found to be x= 2.4, 1.8, 1.2, and 0.7 for samples with target concentrations of x=2, 1.5, 1, and 0.5, respectively. For all compositions found by EDS, the copper plus dopant concentration was always found to be within the naturally occurring range of 12-14.5 with an average of ~12% above the target (12 metal atoms per formula unit). It is noteworthy that the Ag x=2 sample is the

only one in which the actual amount of dopant incorporated is less than the target composition. This was found to be reproducible and is hypothesized to be due to the large ionic radius of Ag^+ (~110 pm) versus the other first row transition metal (II) ions (60-75 pm).[48]

While this study mainly explores dopants for copper, this solution-phase method demonstrated the successful incorporation of Te for Sb ($Cu_{12}Sb_{3.8}Te_{0.2}S_{13}$) and Se for S ($Cu_{12}Sb_4Se_{0.25}S_{12.75}$). Additionally, double substitution has been demonstrated with Zn doped for Cu and Se for S ($Cu_{11}ZnSb_4SeS_{13}$). This is the first time that these tetrahedrite compositions have been synthesized by a solution-phase method. XRD showed high-purity products (Figure 1c), and EDS confirmed compositions consistent with tetrahedrite (Table 1). The actual dopant composition for samples with Te for Sb and Se for S matches well with the target composition, while the Zn for the Cu is enriched consistent with the $Cu_{11}ZnSb_4S_{13}$ sample. This result is expected, as unfilled Cu interstitial spaces are available for enrichment, while no such vacancies are present for Sb and S.[22, 43, 44] Therefore, these findings support the fluctuation for the Cu stoichiometric amount in comparison to the more stable stoichiometric range for Sb and S. Doping of tetrahedrite nanoparticles enables the band gap to be tuned for photovoltaic applications.[5-9, 11, 23, 27]

The broad shape of the XRD peaks is indicative of nanostructured materials produced by this solution-phase method. To investigate the shape and size of the samples produced, TEM and SEM characterization was conducted (Figure 2). TEM images (Figure 2a,b) show the particle size for undoped and doped samples to be between 50 and 200 nm. The representative SEM image shown in Figure 2c demonstrates this size range for a large number of particles. It is noteworthy that these nanoparticles do not have an organic capping layer or shell because this is a surfactant- and ligand-free synthesis. To control particle size and shape, the majority of solution-phase

methods used to produce nanomaterials require this capping layer,[3, 6, 9, 31, 32, 35] which negatively affects thermoelectric properties.[35] Nanoparticles without this organic layer are key for the improvement of thermoelectric properties by decreasing thermal conductivity, as shown previously.[33, 34]

It is worth noting that for the incorporation of all the aforementioned dopants, the reaction temperature was optimized at 220 °C for 1 hour to produce high-purity, ligand-free nanostructured product on the gram-scale. For all syntheses, starting reagents were added in stoichiometric ratios according to the target composition and yet the elemental composition by EDS shows that the Cu (and dopants for Cu) are enriched above this target. While the elemental composition of all products is consistent with the commonly found synthetic range of tetrahedrite ($Cu_{12-14.5}Sb_{4-4.5}S_{13}$), the ability to reduce this copper and associated dopant concentration may enable even greater control over properties relevant for their incorporation in thermoelectric or photovoltaic applications.

Reaction Pathways

The reaction pathway for the formation of undoped and doped tetrahedrite nanomaterials by the modified polyol process was investigated to further understand the phenomenon of copper enrichment in synthetic tetrahedrites. To identify key intermediates, reaction temperatures between room temperature and 250 °C were investigated by heating the reaction mixture to each respective temperature and holding it there for 1 hour. By holding the temperature for this length of time, intermediates formed at those temperatures are able to crystallize for identification. For additional verification of this pathway, the reaction was heated to the optimized temperature of 220 °C and held for less than one hour to confirm that key intermediates were identified. Resulting powders formed at these different temperatures and times were investigated by XRD and EDS.

For investigation of the reaction progress as a function of temperature for undoped tetrahedrite, nanoparticle powder from reactions run between room temperature and 250 °C were characterized by XRD (Figure 3). At room temperature after an hour of stirring, the powder retrieved was primarily amorphous, and this remained the case for all temperatures until 100 °C. At 100 and 150 °C, the intermediates formed are digenite ($Cu_{1.8}S$),[40] covellite (CuS),[39] and valentinite (Sb_2O_3).[41] At 175 °C, famatinite (Cu_3SbS_4)[38] forms and digenite remains. From these two intermediates, tetrahedrite begins to form at 200 °C and is found along with famatinite and digenite. At 215 °C, a significant amount of tetrahedrite is created with the two key intermediates of famatinite and digenite remaining present, which are also notably common impurities for synthetic tetrahedrite.[23, 24, 32, 46] At 220 °C, the intermediates are no longer observed and only tetrahedrite is obtained. When higher temperatures are investigated (250 °C shown in Figure 3), famatinite is formed.

The reaction pathway was also investigated when a dopant was added, specifically the formation of $Cu_{11}ZnSb_4S_{13}$. No change in how the reaction progresses was observed. The addition of a dopant did not alter the growth mechanism (Figure S1). It is anticipated that this result will be consistent for all the diverse compositions shown in this paper because high quality tetrahedrite is produced under identical reaction conditions.

To further explore the reaction pathway, the formation of intermediates as a function of time at the optimized reaction temperature of 220 °C was investigated (Figure 4). After the 30 min ramp from room temperature to 220 °C, the reaction was held at this temperature for 1 min. Famatinite has formed along with all the other intermediates (digenite, valentinitie, and covellite). When the reaction was held at 220 °C for 30 min, tetrahedrite was the dominant species with famatinite, digenite, and valentinite present at low levels. These findings correlate well with the

temperature study. The reaction progresses with Cu-S phases created first, then Sb is incorporated to form famatinite while some digenite remains, and finally pure tetrahedrite is produced.

EDS data reveals the amount of each elemental component that has been incorporated within the solid product as a function of reaction temperature or time (Tables S2-S4). The standard deviation in the spot-to-spot EDS is lowest at the optimized conditions of 220 °C held at 1 hour, which is congruent with the pure-phase XRD data. At 220 °C, the composition of Cu is within the range of tetrahedrite, $Cu_{12\text{-}14.5}Sb_{4\text{-}4.5}S_{13}$. Yet at all other temperatures studied, the amount of Cu recovered is in excess of this range. Additionally, the amount of sulfur retrieved from the reactions below 200 °C is low. It may be that the sulfur is volatilized during the reaction or that unreacted sulfur dissolved within the supernatant is removed during the washes by centrifugation. For the sample collected at 220 °C and only held for 1 min, EDS data shows all elemental compositions within the range of tetrahedrite compositions with low standard deviations regarding spot-to-spot variation. However for the reaction at 220 °C held for 30 min, the composition of Cu was elevated above the target range, S was below the target range, and Sb remained within this range. Large standard deviations nearing 10% were observed after 30 min, representing heterogeneity in the powder sample due to the presence of tetrahedrite, famatinite, valentinite, and digenite. For the undoped tetrahedrite, this heterogeneity was reduced to ~0.5% at the optimized reaction temperature and time of 220 °C for 1 hour, which supports the formation of phase-pure tetrahedrite.

The fact that the copper content of the tetrahedrite is routinely enriched is consistent with the abundance of copper found in the reaction mixture relative to sulfur throughout the reaction progress. Attempts to alter the synthesis by adding more sulfur or decreasing copper resulted in impurities in the final product, namely famatinite and digenite. This is a common impurity found in the literature and found in samples not run under optimized reaction conditions.[23, 24, 32, 46]

Research here has shown that these impurities are key intermediates for the formation of tetrahedrite. It was found that digenite could be selectively etched by sonication in dilute sulfuric acid. Additionally for samples with small famatinite impurities, the impurity was found to be removed by reheating the powder in the solvent tetraethylene glycol for 1 hour at 220 °C similar to previously published solution-phase annealing for this transition.[5] Thus, the idea of tailoring the chemical composition by undertaking this annealing reaction with other reagents, specifically sulfur, present was attempted. Sulfur powder was added into TEG with a pure sample of tetrahedrite for 1 hour at 220 °C. Independent of the amount of sulfur powder added, a famatinite impurity was found consistent with the conversion of tetrahedrite to famatinite upon exposure to sulfur vapor.[6] However, this method may be successful with alternative sulfur sources, such as thiourea and sodium sulfide.

This study shows the evolution of the chemical phases necessary for the formation of pure tetrahedrite by a modified polyol process. Synthesis of binary sulfide compounds (e.g., copper sulfide and antimony sulfide) relevant for solar energy applications has been demonstrated to be feasible by this method.[49-52] The ternary famatinite (Cu_3SbS_4), which is an active area of research for photovoltaic applications,[5, 6, 12] can also be produced by the modified polyol method. The crystal structures of famatinite and tetrahedrite are similar in their atomic arrangement, but tetrahedrite has a larger and more complex unit cell containing 58 atoms versus the 16 atoms found in famatinite.[15, 38] It is interesting that famatinite has a larger ratio of S to Cu than the tetrahedrite, and yet, the tetrahedrite resulting from the famatinite intermediate is copper enriched. However, the tetrahedrite crystal structure ($Cu_{12}Sb_4S_{13}$) is known to contain interstitial sites, in which the additional Cu atoms can be located to produce the enriched tetrahedrite composition of $Cu_{14.5}Sb_4S_{13}$.[22, 43, 44] Regarding the observation of valentinite (Sb_2O_3), it is likely that elemental

Sb nanoparticles formed during the reaction and the oxide subsequently formed during the cleaning centrifugation. Additionally, it is possible that this may have occurred during the reaction at the lower temperatures due to the presence of oxygen in the polyol and acetate counter anions. Previously, the formation of an oxide intermediate has been observed in polyol synthesis, if there are oxygens in the counter anion.[53] In that case, the oxide intermediate was reduced at elevated temperatures as the reducing power of the polyol increases when temperature increases. Note that antimony (III) acetate is preferred for the synthesis over other antimony (III) salts because it is less hygroscopic allowing for more accurate weighing, which is key for the stoichiometric ratios used for the reaction. With this knowledge regarding the reaction growth pathway, research will continue to investigate the means by which the copper concentration can be modified as appropriate for tuning the optical and electrical properties of tetrahedrite.

Thermal Analysis

Thermal analysis by DSC and TGA was conducted from 325-825 K for nanoparticle samples for the undoped tetrahedrite as well as for all other dopants for Cu. This type of characterization has been done for solid-state samples with similar dopant types,[23, 24, 37] but it has not been carried out for samples made by solution-phase methods to produce nanostructured material. Nanostructuring of material by this method has previously been shown to reduce the thermal conductivity of the material and improve the thermoelectric figure of merit.[32-34, 54] While this decrease in size dimensions is favorable for scattering the phonons, it is important to understand the impact on thermal properties. It is anticipated that thermally-induced physical changes on the nanopowders will occur at reduced temperatures relative to bulk powders produced by solid-state methods.

For the undoped tetrahedrite, DSC and TGA data were collected for three samples as shown in Figure 5a. First, the nanopowder as-synthesized was tested. Second, measurements were taken for the sample after being processed by SPS to form a pellet for thermoelectric characterization, which has been shown to maintain the nanoscale grain structure.[33] Third for parallel characterization to the SPS processed sample, a second heat ramp on the DSC and TGA was collected for the nanopowder as-synthesized. In all three cases, an endothermic transition occurred at ~750 K. This same type of transition is seen for tetrahedrite fabricated by solid-state methods, but the transition for that bulk material occurs at ~880 K.[37] It is noteworthy that for tetrahedrite synthesized by both solid-state and solution-phase methods, this transition occurs above the max temperature (~720 K) at which thermoelectric performance is typically characterized for tetrahedrite. Additionally, a small transition occurs at ~425 K. This transition is consistent with what has been observed by others for copper-rich tetrahedrite that typically consist of two related tetrahedrite-type phases with different copper concentrations that coalesce into a single phase at ~400 K.[22] Additionally, it is hypothesized that these two phases may have been more significant in the as-synthesized undoped tetrahedrite sample resulting in the two overlapping transitions at ~750 K. This feature was reproducible and found for multiple as-synthesized undoped tetrahedrite samples. After heat treatment, only a single transition is observed at ~750 K for both the sample processed by SPS and the sample that underwent the second heat ramp in the DSC. For both of these samples, the small transition at ~425 K persisted. This result suggests that the annealing may have made the undoped tetrahedrite more uniform, but the copper-enrichment and associated exsolution transition of the two tetrahedrite-phases at ~425 K remained. Thermal gravimetric analysis showed that the as-synthesized sample exhibited mass loss beginning at ~675 K. However after this loss during the first heat, the sample was more stable during the second heat, as observed

by TGA. The TGA data was consistent for the SPS pellet processed sample and the heat cycle sample with minimal mass loss beginning around 800 K. For the solid-state samples that were similarly pellet processed, a decrease in mass is seen around this same temperature.[23, 24, 37]

Tetrahedrite compounds containing first row transition metal dopants (Zn, Fe, Ni, Co) for Cu did not show an endothermic transition by DSC at ~750 K or within the range measured (325-825 K) for either the x=1 or x=2 dopant concentration. However, the same small transition at ~425 K is observed for these doped samples just as was found for the undoped sample, which is consistent with all samples being copper-enriched. Representative data for the cobalt-doped samples is shown in Figure 5b. The addition of the dopant has increased the thermal stability of the sample and likely increased the endothermic transition to a temperature above the testing range of the instrument. This is consistent with previous reports that indicate dopants for Cu stabilize the tetrahedrite structure.[23, 24, 37] For doped tetrahedrite samples made by solid-state methods, an increase in the temperature at which the endothermic transition occurs was observed to change from 880 K for the undoped to above 900 K for first row transition metal dopants.[37] For all doped samples, the mass loss observed by TGA was less than that of the undoped tetrahedrite. However, a similar mass loss beginning at ~675K was observed for these as-synthesized doped samples, but to a lesser degree. The addition of the dopants seems to decrease the volatility of the sample and increase thermal stability.

For the Ag-doped tetrahedrite, an endothermic transition is observed at a lower temperature relative to the copper-based tetrahedrite (Figure 5c). This transition occurs at a lower temperature for the x=2 sample relative to the x=1. It is hypothesized that the endothermic transition seen at ~750 K for the copper-based sample has been decreased to ~650 K due to the addition of the Ag dopant. While the size of the first row transition metal (M^{2+}) dopants (~60-75 pm) is on par with

the copper (~70-80 pm), the Ag^+ is larger (~110 pm) and is likely decreasing the thermal stability of the material.[48] This conclusion is supported by the finding that the sample with higher Ag concentration demonstrates a transition peak in the DSC data at lower temperature. While the endothermic transition was observed by DSC at a lower temperature, the TGA data for this sample was consistent with the other doped-tetrahedrite samples.

In summary, the nanostructuring of the undoped tetrahedrite does alter the thermal stability of the compound to induce thermal transitions at temperatures lower than those observed for undoped tetrahedrite prepared by solid-state methods. The doping of tetrahedrite with first row transition metals for the Cu stabilized the material by removing the endothermic transition observed at ~750 K, presumably to temperatures beyond the maximum measurement at 825 K. This finding is consistent with what has been found for doped tetrahedrites in the literature.[37] While the temperature for the endothermic transition for the Ag-tetrahedrite was lowered for both composition levels (with the higher dopant level leading to a lower transition temperature), it is interesting that an increase in mass loss by TGA was not associated with these compounds. It would be worthwhile to correlate these findings for the novel Ag-doped tetrahedrite with thermoelectric performance evaluation to see if the transition affects thermoelectric properties. Future experiments will investigate higher temperatures by DSC to determine at what temperature the transitions occur for the first row transition metals and to investigate the effects of dopant concentrations as the Ag-tetrahedrite data suggests.

Conclusions

With the capability of incorporating a range of dopants with tunable concentrations, tetrahedrite nanomaterials can be synthesized by a solution-phase process that is more energy and time efficient than conventional solid-state techniques. For all compounds synthesized, a copper-

enriched tetrahedrite composition, within the typical range of $Cu_{12-14.5}Sb_{4-4.5}S_{13}$, was observed. Investigation of the bottom-up nanomaterial formation by EDS revealed that this is consistent with copper enrichment found in powders collected at all stages of the reaction progress. Key intermediates identified within the growth process are associated with common impurities found in the literature for tetrahedrite synthesized by solid-state and solution-phase methods. Thermal stability studies for these samples showed that the nanostructured materials produced by the modified polyol method have lower thermal stability than the bulk, but the nanomaterial is stable below the typical range at which tetrahedrite is investigated. Additionally, the incorporation of first row transition metal dopants within the compound increased thermal stability.

This research focused on tailoring the concentration of dopants for Cu with doping also demonstrated for Sb and S, as well as doping for multiple elements simultaneously. Within the synthetic versatility study, six tetrahedrite compositions not previously demonstrated by solution-phase techniques have been achieved by the facile synthetic method described herein. Nanostructured material is produced on the gram scale in a single batch via this surfactant- and ligand-free synthetic method. The solution-phase reaction pathway studies identified digenite, covellite, and valentinite as the first intermediates produced. Throughout the reaction, these species are converted to famatinite with digenite remaining. Finally, tetrahedrite is produced at the optimized reaction temperature (220 °C) and time (ramp 30 min, hold 1 hr). These optimized conditions were consistent for all compounds represented here. An investigation of the pathways for the undoped and Zn-based tetrahedrite demonstrated that these pathways were similar, suggesting that the evolution of phases in tethradrite synthesis do not depend on dopant incorporation. The key intermediates preceding the formation of tetrahedrite (famatinite and

digenite) are the most common impurities found for synthetic tetrahedrite samples reported previously.

Nanostructuring and doping were shown to impact the thermal stability of the tetrahedrite compounds, as shown by DSC and TGA. The undoped compound had an endothermic transition at ~750 K, which is less than that observed for bulk material at ~880 K.[37] This endothermic transition for the first row transition metal dopants for Cu was not observed below the 825 K maximum temperature tested. This is consistent with thermal stability studies for tetrahedrite synthesized by solid-state methods that showed dopants increased the temperature at which the endothermic transition occurred by ~50+ degrees. The Ag-doped tetrahedrite had an endothermic transition that occurred at a lower temperature (~650 K) relative to the undoped compound. The significantly larger ionic radius of the Ag^{+} relative to the first row transition metals likely destabilizes the compound with the larger dopant concentration of Ag^{+}, resulting in an endothermic transition at a slightly lower temperature. For all compounds, a transition was observed at ~400 K, which is consistent with a copper-enriched tetrahedrite compound. TGA for all compounds showed a decrease in mass that began at ~675 K with the as-synthesized undoped tetrahedrite having a greater mass loss. This mass loss is likely due to the vaporization of sulfur, but could also be due to residual organic solvent from the synthesis. This is unlikely because the more significant mass loss was observed only for the undoped sample and therefore is most likely due to undoped sample being less thermally stable. However after this as-synthesized sample undergoes a heat treatment (or pellet processing by SPS), the thermal stability measured by TGA is improved and becomes comparable to the doped tetrahedrite samples. For the as-synthesized undoped tetrahedrite, the endothermic transition observed by DSC at ~750K persisted at the same temperature after heat treatment.

Understanding the synthetic versatility, reaction pathway, and thermal stability for the solution-phase formation of tetrahedrite nanomaterials is relevant for their future incorporation in thermoelectric and photovoltaic applications. Future research will investigate temperatures above 825 K to confirm that the endothermic transition for the first row transition metals was elevated and not eliminated. Additionally, this will investigate if the dopant level also impacts the temperature at which this transition occurs. Further exploration of the growth mechanism and sample stability could be explored via in-situ high-temperature XRD. Optimization of the synthetic procedure to control the Cu concentration (reduce the Cu enrichment) will be a focus of future research. This synthetic method and study of the reaction pathway presents insight necessary to tune the concentration and expand the different types of dopants incorporated, enabling material properties (e.g., band gap, thermopower, etc.) to be tailored for optimal performance in renewable energy technologies.

Conflicts of Interest

There are no conflicts of interest to declare.

Acknowledgements

Aspects of this work were supported by NSF EPSCoR MADE in SC Program Award #OIA-1655740, NSF-CHE 1905221, NSF-CBET 1507789, and U.S. Dept. of Education Graduate Assistantships in Areas of National Need (GAANN) Award P200A140215. Christine D. Fasana and Grace E. Kunkel were supported by the Arnold and Mabel Beckman Foundation Scholars Program. Additional funding was provided by Furman University Chemistry departmental funds and the Schaap Endowed Fund for Undergraduate Research at Hope College. For technical

assistance, we thank Cameron Holder, Jennifer Misuraca from JEOL USA Inc., and the Pennsylvania State University's MRI MCL.

Supporting Information

Calculated lattice constants for all tetrahedrite compositions. XRD and EDS data associated with reaction pathway for synthetic tetrahedrite compounds.

References

1 A. V. Powell, *J. Appl. Phys.,* 2019, **126,** 100901(1-19).

2 R. Chetty, A. Bali and R. C. Mallik, *J. Mater. Chem. C,* 2015, **3,** 12364-12378.

3 K. Ramasamy, H. Sims, W. H. Butler and A. Gupta, *Chem. Mater.,* 2014, **26,** 2891-2899.

4 S. A. McClary, R. B. Balow and R. Agrawal, *J. Mater. Chem. C,* 2018, **6,** 10538-10546.

5 S. Suehiro, K. Horita, M. Yuasa, T. Tanaka, K. Fujita, Y. Ishiwata, K. Shimanoe and T. Kida, *Inorg. Chem.,* 2015, **54,** 7840-7845.

6 J. van Embden, K. Latham, N. W. Duffy and Y. Tachibana, *J. Am. Chem. Soc.,* 2013, **135,** 11562-11571.

7 C. Coughlan, M. Ibáñez, O. Dobrozhan, A. Singh, A. Cabot and K. M. Ryan, *Chem. Rev.,* 2017, **117,** 5865-6109.

8 C. Tablero, *J. Phys. Chem. C,* 2014, **118,** 15122-15127.

9 M. Tamilselvan and A. J. Bhattacharyya, *ACS Appl. Mater. Inter.,* 2018, **1,** 4227-4234.

10 J. Heo, R. Ravichandran, C. F. Reidy, J. Tate, J. F. Wager and D. A. Keszler, *Adv. Energy Mater.,* 2015, **5,** 1401506(1-7).

11 K. Chen, J. Zhou, W. Chen, P. Zhou, F. He and Y. Liu, *Part. Part. Syst. Char.,* 2015, **32,** 999-1005.

12 C. T. Crespo, *J. Phys. Chem. C,* 2016, **120,** 7959-7965.

13 L. E. Bell, *Science,* 2008, **321,** 1457-1461.

14 T. M. Tritt, *Annu. Rev. Mater. Res.,* 2011, **41,** 433-448.

15 B. J. Wuensch, *Z. Kristallogr. NCS,* 1964, **119,** 437-453.

16 W. Lai, Y. Wang, D. T. Morelli and X. Lu, *Adv. Funct. Mater.,* 2015, **25,** 3648-3657.

17 G. Tan, L. Zhao and M. G. Kanatzidis, *Chem. Rev.,* 2016, **116,** 12123-12149.

18 G. J. Snyder and E. S. Toberer, *Nature Materials,* 2008, **7,** 105-114.

19 J. P. Heremans, M. S. Dresselhaus, L. E. Bell and D. T. Morelli, *Nat. Nanotechnol.,* 2013, **8,** 471-473.

20 M. G. Kanatzidis, *Chem. Mater. ,* 2010, **22,** 648-659.

21 K. Biswas, J. He, I. D. Blum, C. Wu, T. P. Hogan, D. N. Seidman, V. P. Dravid and M. G. Kanatzidis, *Nature,* 2012, **489,** 414-418.

22 P. Vaqueiro, G. Guélou, A. Kaltzoglou, R. I. Smith, T. Barbier, E. Guilmeau and A. V. Powell, *Chem. Mater.,* 2017, **29,** 4080-4090.

23 S. Tippireddy, R. Chetty, M. H. Naik, M. Jain, K. Chattopadhyay and R. C. Mallik, *J. Phys. Chem. C,* 2018, **122,** 8735-8749.

24 T. Barbier, P. Lemoine, S. Gascoin, O. I. Lebedev, A. Kaltzoglou, P. Vaqueiro, A. V. Powell, R. I. Smith and E. Guilmeau, *J. Alloys Compd.,* 2015, **634,** 253-262.

25 X. Lu, D. T. Morelli, Y. Xia, F. Zhou, V. Ozolins, H. Chi, X. Zhou and C. Uher, *Adv. Energy Mater.,* 2013, **3,** 342-348.

26 X. Lu, D. T. Morelli, Y. Xia and V. Ozolins, *Chem. Mater.,* 2015, **27,** 408-413.

27 J. Heo, G. Laurita, S. Muir, M. A. Subramanian and D. A. Keszler, *Chem. Mater.,* 2014, **26,** 2047-2051.

28 Weller, Daniel P., Morelli, Donald T., *J. Alloys Compd.,* 2017, **710,** 794-799.

29 T. Barbier, S. Rollin-Martinet, P. Lemoine, F. Gascoin, A. Kaltzoglou, P. Vaqueiro, A. V. Powell and E. Guilmeau, *J. Am. Ceram. Soc.,* 2016, **99,** 51-56.

30 S. Bera, A. Dutta, S. Mutyala, D. Ghosh and N. Pradhan, *J. Phys. Chem. Lett.,* 2018, **9,** 1907-1912.

31 T. Nakada, M. Takahashi, C. Shijimaya, K. Higashimine, W. Zhou, P. Dwivedi, M. Ohta, H. Takida, T. Akatsuka, M. Miyata and S. Maenosono, *Langmuir,* 2019, **35,** 16335-16340.

32 D. J. James, X. Lu, D. T. Morelli and S. L. Brock, *ACS Appl. Mater. Inter.,* 2015, **7,** 23623-23632.

33 D. P. Weller, D. L. Stevens, G. E. Kunkel, A. M. Ochs, C. F. Holder, D. T. Morelli and M. E. Anderson, *Chem. Mater.,* 2017, **29,** 1656-1664.

34 D. P. Weller, G. E. Kunkel, A. M. Ochs, D. T. Morelli and M. E. Anderson, *Mater. Today Phys.,* 2018, **7,** 1-6.

35 M. E. Anderson, S. S. N. Bharadwaya and R. E. Schaak, *J. Mater. Chem,* 2010, **2,** 8362-8367.

36 F. Fiévet, S. Ammar-Merah, R. Brayner, F. Chau, M. Giraud, F. Mammeri, J. Peron, J. Y. Piquemal, L. Sicard and G. Viau, *Chem. Soc. Rev.,* 2018, **47,** 5187-5233.

37 J. Pi, G. Lee and I. Kim, *J. Electron. Mater,* 2020, **49,** 2710-2718.

38 J. Garin and E. Parthé, *Acta Cryst. B,* 1972, **28,** 3672-3674.

39 Y. Takéuchi, Y. Kudoh and G. Sato, *Z. Kristallogr. Cryst. Mater.,* 1985, **173,** 119-128.

40 K. Yamamoto and S. Kashida, *J. Solid State Chem.,* 1991, **93,** 202-211.

41 J. D. Hanawalt, H. W. Rinn and L. K. Frevel, *Ind. Eng. Chem. Anal. Ed.,* 1938, **10,** 457-512.

42 Tatsuka, Kiyoaki, Borimoto, Nobuo, *Am. Mineral.,* 1973, **58,** 425-434.

43 N. Ghassemi, X. Lu, Y. Tian, E. Conant, Y. Yan, X. Zhou and J. H. Ross, *ACS Appl. Mater. Inter.,* 2018, **10,** 36010-36017.

44 N. Ghassemi, Y. Tian, X. Lu, Y. Yan, X. Zhou and J. H. Ross, *J. Phys. Chem. C,* 2020, **124,** 3973-3979.

45 J. A. Mielczarski, J. M. Cases, M. Alnot and J. J. Ehrhardt, *Langmuir,* 1996, **12,** 2531-2543.

46 S. Harish, D. Sivaprahasam, M. Battabyal and R. Gopalan, *J. Alloys Compd.,* 2016, **667,** 323-328.

47 R. Chetty, A. Bali, M. H. Naik, G. Rogl, P. Rogl, M. Jain, S. Suwas and R. C. Mallik, *Acta Mater.,* 2015, **100,** 266-274.

48 R. D. Shannon, *Acta Crystallogr A.,* 1976, **32,** 751-767.

49 Y. Liu and A. R. Hight Walker, *J. Phys. Chem. B,* 2010, **114,** 4264-4271.

50 D. Mott, J. Yin, M. Engelhard, R. Loukrakpam, P. Chang, G. Miller, I. Bae, N. Chandra Das, C. Wang, J. Luo and C. Zhong, *Chem. Mater.,* 2010, **22,** 261-271.

51 R. Zhang, X. Chen, M. Mo, Z. Wang, M. Zhang, X. Liu and Y. Qian, *J. Cryst. Growth,* 2004, **262,** 449-455.

52 Y. Yu, R. H. Wang, Q. Chen and L. M. Peng, *J. Phys. Chem. B,* 2006, **110,** 13415-13419.

53 C. F. Holder, E. E. Rugen and M. E. Anderson, *Nanomater. Energy,* 2014, **3,** 206-214.

54 H. Hu, F. Sun, J. Dong, H. Zhuang, B. Cai, J. Pei and J. Li, *ACS Appl. Mater. Inter.,* 2020, **12,** 17852-17860.

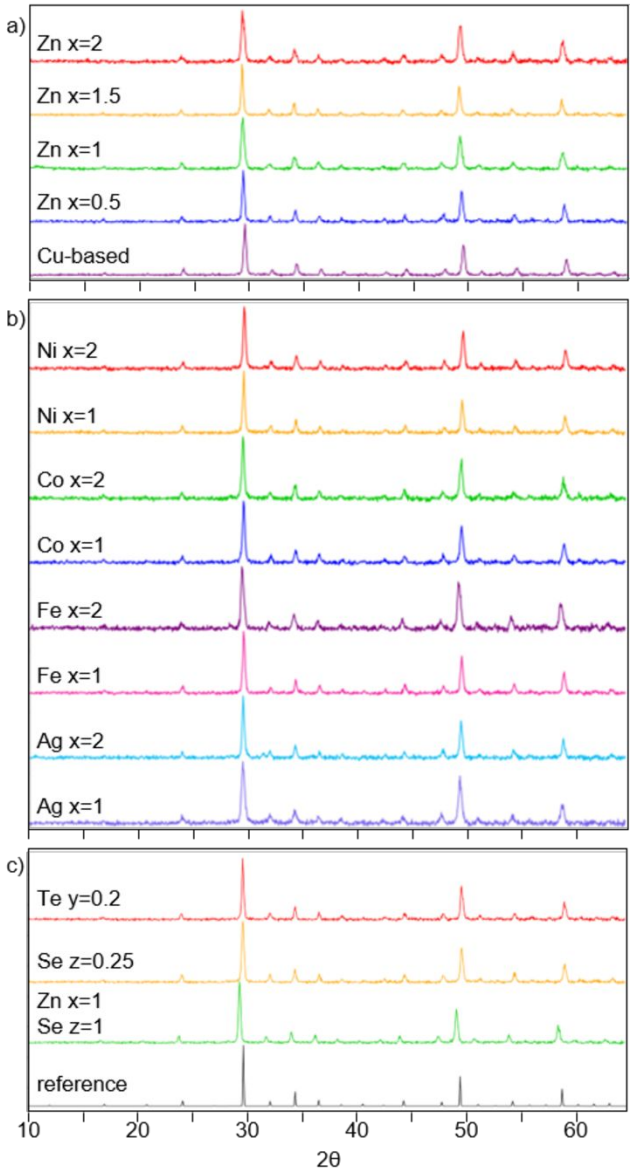

Figure 1. XRD patterns collected for a variety of tetrahedrite samples synthesized by modified polyol process: a) Undoped and Zn-doped tetrahedrite ($Cu_{12-x}Zn_xSb_4S_{13}$) samples, b) Ni-, Co-, Fe-, and Ag-doped tetrahedrite ($Cu_{12-x}M_xSb_4S_{13}$ with dopant=M) samples, and c) Te-substituted tetrahedrite, Se-substituted tetrahedrite, and doubly substituted Zn-doped and Se-substituted tetrahedrite ($Cu_{12-x}M_xSb_{4-y}M_yS_{13-z}M_z$ samples). Reference pattern for tetrahedrite found in c.[15]

Table 1. Elemental analysis of tetrahedrite compounds by EDS. Average atomic ratios given with standard deviation. Atomic ratios determined relative to S, which was normalized to 13 S atoms per formula unit. In the case of multiple dopants, the first dopant to appear in the target composition is listed first.

Target Composition	Cu	Sb	S	Dopant
$Cu_{12}Sb_4S_{13}$	13.4±0.3	4.4±0.2	13.0±0.3	
$Cu_{10}Zn_2Sb_4S_{13}$	11.2±0.3	3.9±0.2	13.0±0.2	2.40±0.03
$Cu_{10.5}Zn_{1.5}Sb_4S_{13}$	11.7±0.3	4.0±0.2	13.0±0.2	1.80±0.02
$Cu_{11}ZnSb_4S_{13}$	12.0±0.4	4.04±0.04	13.0±0.5	1.21±0.07
$Cu_{11.5}Zn_{0.5}Sb_4S_{13}$	12.42±0.05	3.92±0.07	13.0±0.5	0.71±0.02
$Cu_{10}Ni_2Sb_4S_{13}$	12.3±0.3	4.5±0.2	13.0±0.2	2.32±0.05
$Cu_{11}NiSb_4S_{13}$	12.9±0.1	4.40±0.05	13.0±0.2	1.17±0.02
$Cu_{10}Co_2Sb_4S_{13}$	11.7±0.2	4.20±0.03	13.0±0.2	2.02±0.02
$Cu_{11}CoSb_4S_{13}$	12.99±0.09	4.34±0.02	13.0±0.1	1.37±0.03
Cu_{10} $Fe_2Sb_4S_{13}$	10.5±0.7	4.1±0.3	13.0±0.5	2.1±0.2
$Cu_{11}FeSb_4S_{13}$	11.6±0.2	4.1±0.1	13.0±0.3	1.07±0.02
$Cu_{10}Ag_2Sb_4S_{13}$	11.6±0.2	3.8±0.2	13.0±0.2	1.78±0.08
$Cu_{11}AgSb_4S_{13}$	12.8±0.5	4.3±0.1	13.0±0.3	1.0±0.2
$Cu_{12}Sb_{3.8}Te_{0.2}S_{13}$	14.5±0.3	3.70±0.05	13.0±0.2	0.21±0.01
$Cu_{12}Sb_4Se_{0.25}S_{12.75}$	13.3±0.2	4.1±0.1	12.7±0.1	0.23±0.04
$Cu_{11}ZnSb_4SeS_{13}$	12.37±0.09	4.44±0.04	12.08±0.09	1.17±0.05 0.91±0.06

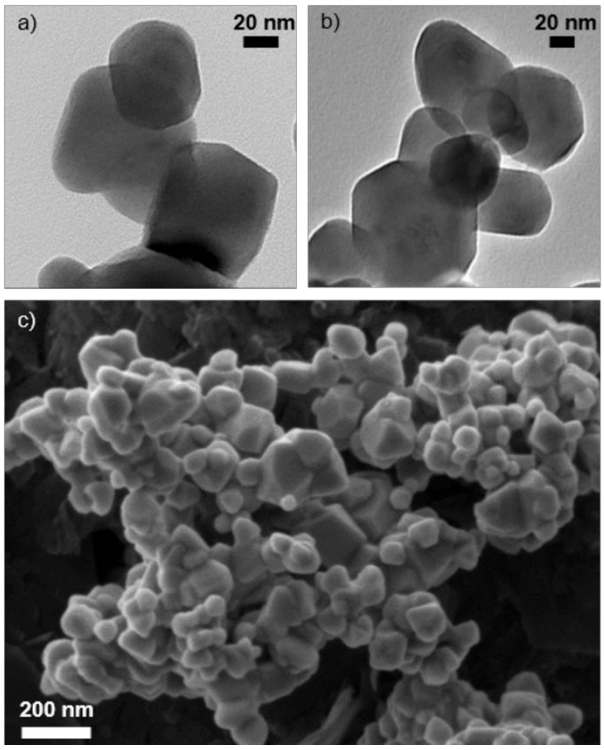

Figure 2. TEM images of a) undoped and b) Zn x=1 doped tetrahedrite samples. SEM image of c) undoped tetrahedrite powder. Particle sizes range from 50-200 nm.

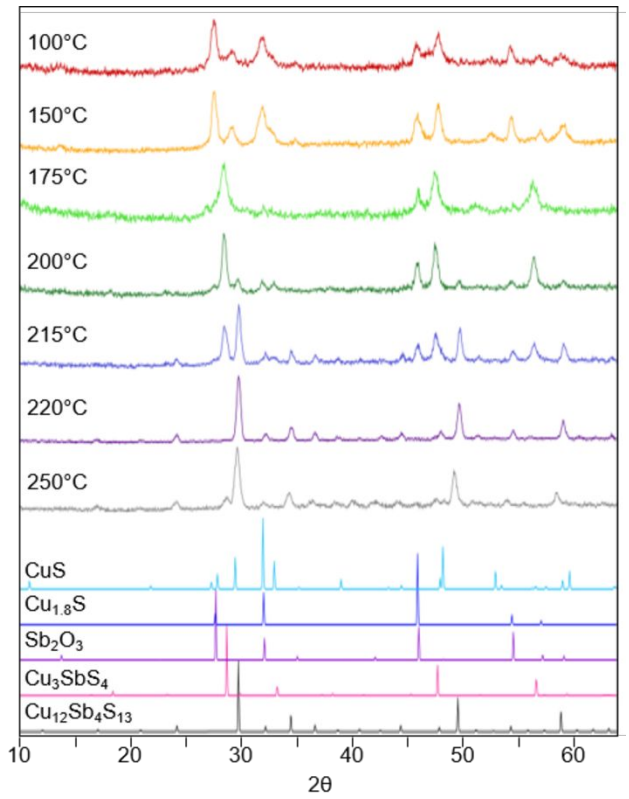

Figure 3. XRD patterns collected for undoped tetrahedrite samples synthesized at different reaction temperatures. Reference patterns provided for tetrahedrite ($Cu_{12}Sb_4S_{13}$),[15] famatinite (Cu_3SbS_4),[38] digenite ($Cu_{1.8}S$),[40] valentinite (Sb_2O_3),[41] and covellite (CuS).[39]

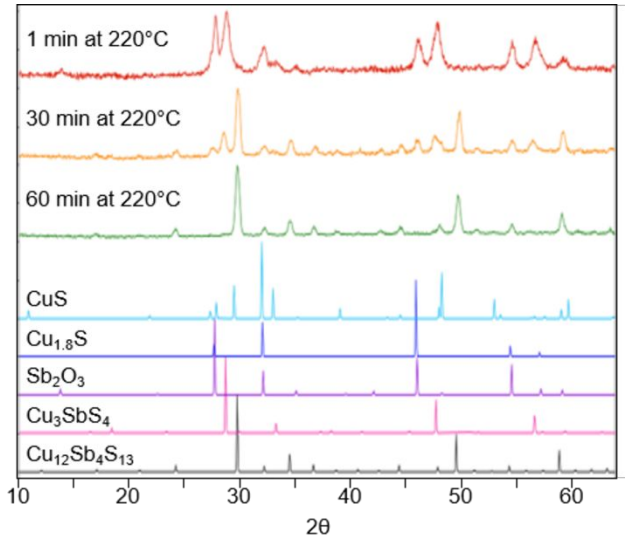

Figure 4. XRD patterns collected for undoped tetrahedrite samples synthesized at the optimized reaction temperature of 220°C for various times. Reference patterns provided for tetrahedrite ($Cu_{12}Sb_4S_{13}$),[15] famatinite (Cu_3SbS_4),[38] digenite ($Cu_{1.8}S$),[40] valentinite (Sb_2O_3),[41] and covellite (CuS).[39]

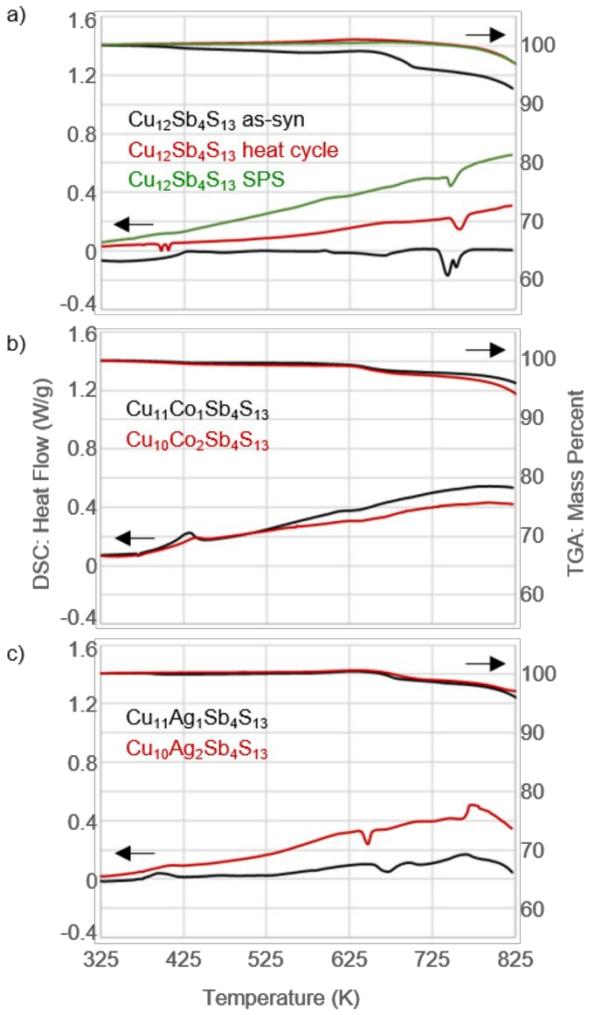

Figure 5. DSC and TGA data for a) undoped tetrahedrite, b) Co-doped tetrahedrite, and c) Ag-doped tetrahedrite. In all graphs, DSC data is plotted at the bottom and associated with left axis and TGA data is plotted at the top and associated with right axis. Arrows are provided on graph for clarity. a) Data provided for undoped tetrahedrite after synthesis (as-syn), after a single heat cycle in the instrument, and after pellet processing by spark plasma sintering (SPS). b,c) Data provided for Co and Ag doped samples after synthesis.

Table of Contents Figure

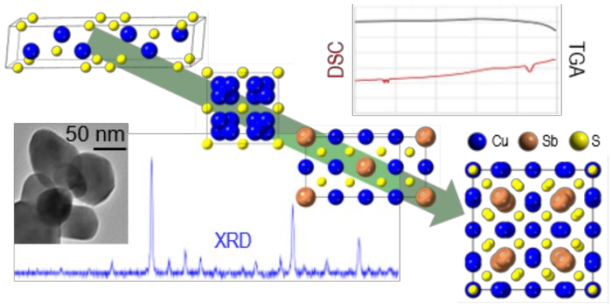

Modified polyol process produces undoped and doped tetrahedrite. Bottom-up solution-phase formation of nanomaterial investigated. Impact of nanostructuring and doping on thermal properties evaluated.